Alma Mater Studiorum Università di Bologna
Archivio istituzionale della ricerca

UNDI: An open-source library to simulate muon-nuclear interactions in solids

09 August 2024

UNDI: an open-source library to simulate muon-nuclear interactions in solids

Pietro Bonfà[a,1], Jonathan Frassineti[b], Muhammad Maikudi Isah[a], Ifeanyi John Onuorah[a], Samuele Sanna[b]

[a]*Dipartimento di Scienze Matematiche, Fisiche e Informatiche, Università di Parma, 43124 Parma, Italy*
[b]*Dipartimento di Fisica e Astronomia, Università di Bologna, 40127 Bologna, Italy*

Abstract

We present UNDI, an open-source program to analyse the time dependent spin polarization of an isolated muon interacting with the surrounding nuclear magnetic dipoles in the context of standard muon spin rotation and relaxation spectroscopy experiments.

The code can perform both exact and approximated estimates of the muon polarization function in presence of external fields and electric field gradients on the nuclei surrounding the muon.

We show that this tool, combined to *ab initio* estimations of the electric field gradient at the nuclei interacting with the muon, can become a valuable complement to supercell based identifications of muon sites in crystals when large nuclear magnetic moments are present in the sample. In addition, it allows to properly investigate physical properties influenced by the presence of a non-negligible electric field gradient such as avoided level crossing resonance, nature of the ground state, disentanglement of electronic and nuclear magnetic moments or charge ordered states.

The efficiency and effectiveness of this method is shown along the lines of three realistic examples.

Keywords: Muon Spin Rotation and Relaxation Spectroscopy; Spin Hamiltonian; Data analysis; Density Functional Theory; Magnetism; Python 3

[*]Corresponding author.
E-mail address: pietro.bonfa@unipr.it

PROGRAM SUMMARY

1. Introduction

Muon spin rotation and relaxation spectroscopy (μSR) is an experimental technique that uses the spin of muons as extraordinary sensitive probes of magnetic fields, capable of detecting down to 10^{-4} T [1]. In magnetic materials it is used in a similar fashion to Nuclear Magnetic Resonance (NMR), but with the notable difference that the muon is injected into the sample already 100% spin polarized. This is a great advantage with respect to NMR since it removes the need for applying external magnetic fields to polarize and perturb the nuclear spins. The time evolution of the muon polarization can be detected by counting the spatial distribution of positrons emitted in the muon decay process, again without the need of detecting a radio-frequency signal as in NMR experiments. In addition, it can be used with virtually any material provided that the muon stops in the target sample. The drawback is that the position occupied by the muon is generally unknown.

In systems with well characterized magnetic order, the occupied site(s) may be identified by comparing the experimental local field with the estimate obtained from the dipolar interaction of the muon with the spin polarized electronic orbitals. This is only possible, however, when the contact hyperfine field at the muon site is known to be negligible.

First principles simulations have been proposed as a general solution and have already been extensively used to tackle this problem [2, 3, 4, 5, 6, 7], but their adoption requires some effort, especially due to the fact that in standard experimental conditions, the muon is an extremely diluted charged

particle in a periodic system. A compromise must be done in order to accurately describe the hosting material and, at the same time, to get rid of the periodicity effects when accounting for muon related properties. This is most commonly done with the supercell approach that still requires non-negligible computational efforts [8, 9].

An alternative method is to exploit the known details of the nuclei surrounding the muon to obtain information on the interstitial positions that it can potentially occupy. These studies must be performed in the paramagnetic phase where magnetic fluctuations of electronic origin average out on the time scale probed by the muon, but, at the same time, in a temperature range where thermally activated muon diffusion does not hinder the dipolar interaction with nuclear magnetic moments. Luckily, this situation is not so uncommon, since thermally activated muon diffusion is very often observed at temperatures higher than magnetic ordering.

This approach has indeed already been pursued and described in literature, with the most common strategy being the adoption of the secular approximation for the dipolar interaction of the muon with the surrounding nuclei in the presence of applied fields. However, an approximated but fast and accurate method to calculate muon polarization functions at full quantum level has been introduced by Celio about 30 years ago and it requires seconds to run on modern hardware[1] [11]. A general and efficient implementation would allow the widespread adoption of this approach to routinely evaluate the nuclear contributions to μSR signals. Despite its simplicity, such a tool is still not available to the general public as an open-source software package to the best of our knowledge.

For this reason we developed and shared UNDI (mUon Nuclear Dipolar Interaction), a program that calculates the polarization function of muons in solids using both exact or approximated solutions based on the method described in Ref. [11]. In addition, in metallic materials, we show that simple *ab initio* based estimates performed on the unperturbed lattice already provide the most relevant contributions to the Hamiltonian describing the muon-sample interaction without having to revert to long supercell simulations [9].

---

[1]The author of Ref. [10] reported that a single calculation took about an hour on a 30 years old VAX 8600 system.

2. Muon-nuclei interaction

The problem that we wish to solve with UNDI is described by the following Hamiltonian:

$$\mathcal{H} = \mathcal{H}_{Z,\mu} + \sum_i^N \mathcal{H}_{Z,i} + \mathcal{H}_{\mathrm{dip},i} + \mathcal{H}_{Q,i} + \sum_{i,j>i}^N \mathcal{H}_{\mathrm{dip},ij} \qquad (1)$$

where the sum extends over N nuclei, and

$$\mathcal{H}_{Z,\mu} = -\hbar\gamma_\mu \mathbf{I}_\mu \cdot \mathbf{B}_{ext} \qquad (2)$$

$$\mathcal{H}_{Z,i} = -\hbar\gamma_i \mathbf{I}_i \cdot \mathbf{B}_{ext} \qquad (3)$$

$$\mathcal{H}_{\mathrm{dip},i} = \frac{\mu_0 \hbar^2}{4\pi}\gamma_i\gamma_\mu \left(\frac{\mathbf{I}_i \cdot \mathbf{I}_\mu}{r^3} - \frac{3(\mathbf{I}_i \cdot \mathbf{r})(\mathbf{I}_\mu \cdot \mathbf{r})}{r^5} \right) \qquad (4)$$

$$\mathcal{H}_{\mathrm{dip},ij} = \frac{\mu_0 \hbar^2}{4\pi}\gamma_i\gamma_j \left(\frac{\mathbf{I}_i \cdot \mathbf{I}_j}{r_{ij}^3} - \frac{3(\mathbf{I}_i \cdot \mathbf{r}_{ij})(\mathbf{I}_j \cdot \mathbf{r}_{ij})}{r_{ij}^5} \right) \qquad (5)$$

$$\mathcal{H}_{Q,i} = \frac{eQ_i}{6I_i(2I_i - 1)} \sum_{\alpha,\beta \in \{x,y,z\}} V_i^{\alpha\beta} \left[\frac{3}{2}\left(I_i^\alpha I_i^\beta + I_i^\beta I_i^\alpha \right) - \delta_{\alpha\beta} I_i^2 \right] \qquad (6)$$

where $\mathcal{H}_{Z,\mu}$ and $\mathcal{H}_{Z,i}$ are the Zeeman interactions for the muon and for each nucleus subject to the field B_{ext}, $\mathcal{H}_{\mathrm{dip},i}$ is the dipolar interaction between the muon and the nuclei and $\mathcal{H}_{\mathrm{dip},ij}$ is the dipolar interaction between the nuclei i and j. Finally, $\mathcal{H}_{Q,i}$ is the quadrupolar interaction, with $\mathbf{V}_i$ being the electric field gradient (EFG) at nuclear site i. In Eqs. 3-6, $\mathbf{I}_i$ is the spin operator of nucleus i, characterized by a the gyromagnetic ratio γ_i, in Eq. 2 $\mathbf{I}_\mu$ is the spin operator of the muon, that has gyromagnetic ratio γ_μ, and $\mathbf{r}$ is the vector from the muon to the various nuclei while $\mathbf{r}_{ij}$ is the distance between nuclei i and j. In general, in light of the r^{-3} decrease in the strength of the dipolar interaction, the sum is limited to a few nearest neighbors of the muon and the dipolar interaction between the various nuclei can often be neglected.

In standard experimental conditions, the nuclear moments are not magnetically ordered and the muon stops inside the sample with a defined initial spin polarization directed as:

$$\mathbf{s}_\mu = \frac{\mathbf{I}_\mu}{I_\mu} \qquad (7)$$

The system can be described by the following density operators:

$$\rho = \rho_\mu \otimes \frac{\mathcal{I}}{D} \tag{8}$$

$$\rho_\mu = \frac{1}{2}\left(\mathcal{I} + \mathbf{s}_\mu \cdot \boldsymbol{\sigma}\right) \tag{9}$$

where $\boldsymbol{\sigma}$ are Pauli operators, $\mathcal{I}$ is the identity operator, $D = \prod_i^N (2I_i + 1)$ and second term in the tensor product of Eq. 8 is a consequence of the weakness of the nuclear interactions with respect to thermal energy.

In the Heisenberg representation, the evolution of the operators representing the muon spin is given by

$$\hbar \frac{\mathrm{d}\boldsymbol{\sigma}(t)}{\mathrm{d}t} = i\left[\mathcal{H}, \boldsymbol{\sigma}(t)\right] \tag{10}$$

and the experimentally acquired data is the projection of the muon spin along a given direction $\mathbf{d}$

$$P(t)_d = \mathrm{Tr}\{\rho\boldsymbol{\sigma}(t) \cdot \mathbf{d}\} \tag{11}$$

In order to correctly reproduce the muon polarization as a function of time, in general, an estimate of the EFG present on the nuclei (with spin larger than one half) interacting with the muon is required. In addition, the muon itself will generate an EFG on the nuclei of the hosting material. The relative importance of this last term with respect to bulk EFG drastically depend on the system under the study. Influencing factors are both the electron density of the system and the amount of distortion introduced by the muon. Independent determinations of the EFGs in the system with NMR measurements or *ab initio* calculations are two strategies that can be used to acquire further information on this point. Here we follow the latter option and we discuss it later with the help of some examples.

When the Hilbert space associated with $\mathcal{H}$ becomes exceedingly large, the approach first proposed by Celio [11], which is based on a Trotter approximation for the computation of the time evolution of an initial state prepared as a random superposition of basis functions, can be used to speedup the simulation. The method has already been described in details and we refer the reader to the original reference or the book by Alain Yaouanc and Pierre Dalmas de Réotier for additional details [12]. Here we provide a very concise

description to present the relevant aspects of the algorithm discussed in the following sections.

First, one notes that, if the last term in Eq. 1 can be neglected, the interaction can be rewritten as

$$\mathcal{H} = \sum_i^N \frac{\mathcal{H}_{\mathrm{Z},\mu}}{N} + \mathcal{H}_{\mathrm{Z},i} + \mathcal{H}_{\mathrm{d}ip,i} + \mathcal{H}_{\mathrm{Q},i} = \sum_i^N \mathcal{H}_i \tag{12}$$

and in this form, the time evolution operator reads

$$\mathcal{U} = \exp\left(-i\frac{\mathcal{H}}{\hbar}t\right) = \lim_{k\to\infty}\left[\prod_{i=1}^N \exp\left(-i\frac{\mathcal{H}_i}{k}\frac{t}{\hbar}\right)\right]^k \tag{13}$$

where the last term in Eq. 13 is the Trotter expansion. In order to avoid the computation of the matrix elements of $\boldsymbol{\sigma}(t)$, the problem is tackled in the Schrödinger picture by evolving in time a wave-function obtained from the following random superposition of the basis states $|u_l\rangle$ of the system:

$$|\phi\rangle = \sum_{l=1}^{d_{\mathcal{H}}/2} \sqrt{\frac{4}{d_{\mathcal{H}}}} e^{i\lambda_l} |u_l\rangle \tag{14}$$

where $d_{\mathcal{H}}$ is the dimension of the Hilbert space and λ_l is chosen at random from a uniform distribution with endpoints $[0, 2\pi)$. It can be shown [11] that, as a consequence of the linearity of the Schrödinger equation, the expectation value of the muon spin on the time evolved states $|\phi\rangle$ is the sum of two contributions, the exact one and an additional term that scales as $1/d_{\mathcal{H}}$ and depends on the initial (random) choice of coefficients λ. This last term averages out after multiple iterations of the algorithm.

Convergence with respect to the number of repetitions to be performed is generally fast (for example, only 4 repetition are needed for the 8192 dimensional Hilbert space of the example on copper discussed below). On current consumer-level hardware, this method becomes faster than full Hamiltonian diagonalization already for matrices of a few hundreds elements' size.

An interesting phenomenon that UNDI allows to simulate is avoided level crossing resonance (ALCR). The topic has been covered extensively in literature and we refer the reader for example to Ref. [13]. In brief, when the Zeeman energy levels generated by a longitudinal external field match the quadrupolar splitting on nuclei with spin one or greater experiencing an EFG, the muon depolarization is enhanced. This is the phenomenon revealed by the various examples discussed in this manuscript.

3. Description of the code

UNDI calculates the muon polarization as a function of time, Eq. 11, assuming the initial muon polarization $\mathbf{s}_\mu$ to be along $\hat{z}$.

As a consequence, an external field applied along the direction of the muon spin polarization, called longitudinal field in μSR nomenclature, should be applied along $\hat{z}$, while a field perpendicular to $\hat{z}$ will represent a so-called transverse field.

Since powder averages are most often required, a function to rotate all quantities defining the sample, namely the atomic coordinates and the EFG tensors, is provided. This simplifies the alignment of a given direction with the initial muon polarization. It is also possible to rotate the initial polarization of the muon, but keeping it fixed simplifies the identification of external fields directions. Indeed the sample rather than the muon polarization and external field is actually rotated in real experiments.

3.1. Dependencies and installation

UNDI is a Python code based on NumPy [14] and QuTip [15, 16], which are both extensively used and actively developed libraries.

The code accepts as an input a list of dictionaries that contain all the details of the system to be simulated. Information about nuclear properties are obtained through the Mendelev python package [17] but all the details can be overridden in order to accommodate, for example, averages over arbitrary isotopical compositions.
The latest stable version of UNDI, version 1.0 at the time of writing, can be installed using the Python Packaging Index (`pip`) with the following command:

```
pip install undi
```

The project's GitHub repository is located at `https://github.com/bonfus/undi`.

3.2. Sample and environment definition

The current version of the code accepts the following input descriptors that should be provided as the keys of a dictionary describing each nucleus in a list of nuclei:

- `Position` : 3D vector, the position of the nucleus or the muon in Cartesian coordinates.

```
# This is a linear F-mu-F along z
r=1.17 * angtom
atoms = [
            {'Position': np.array([0., 0., 0.]),
            'Label': 'F'},
            {'Position': np.array([0., 0., r ]),
            'Label': 'mu'},
            {'Position': np.array([0., 0., 2*r]),
            'Label': 'F'}
        ]
```

Figure 1: Minimal input data for UNDI. This input can be used to reproduce the results presented in Ref. [18] for a linear F-μ-F structure. The variable `angtom` equals 10^{-10} and is used to specify the coordinates in SI units.

- Label : string, this can be either 'mu', a chemical symbol or the isotope name, for example `Al` or `63Cu`.

- Spin : real, the spin of the nucleus or of the muon (optional).

- Gamma : real, the gyromagnetic ratio of the muon/nucleus (optional).

- ElectricQuadrupoleMoment : real, the nuclear quadrupole moment (optional).

- EFGTensor : 3D matrix, the EFG tensor in Cartesian coordinates (optional, default zero).

All details are optional except for the `Label` and the `Position`. Missing information are taken from the Mendelev package and the most abundant isotope is selected by default. A message warns the user when multiple isotopes should be considered or when the potentially interacting nuclei are only a fraction of the natural occurring isotopes (in both cases the threshold is set to 99% relative abundance). All quantities should be provided and are returned by the code in SI units. A self-explanatory example of input data is shown in Fig. 1.

An external field can be applied in any direction. This is shown in the next section.

3.3. Running a simulation

The muon polarization projected along the $\hat{z}$ direction is obtained by first defining the interactions and then computing the expected signal either exactly or with the approximation already introduced.

8

The system is first described by initializing the `MuonNuclearInteraction` class, for example:

```
MNI = MuonNuclearInteraction(nuclei, external_field
    =[0.,0.,0.001])
```

In the previous line we have initialized the system with the set of nuclei contained in the list of dictionaries `nuclei` and a longitudinal external field of 1 mT is applied.

The expected signal is then obtained as

```
signal = MNI.polarization(times)
```

where `times` is a 1D NumPy array containing the list of times to be used for the computation of the muon polarization.

Alternatively, the approximated signal is obtained with

```
signal = MNI.celio(times, k=2)
```

where `k` is the coefficient in the Trotter approximation of Eq. 13. This command should be repeated a number of times depending on the dimension of the Hilbert space. The convergence of the algorithm is discussed in detail with the examples described later.

3.4. Documentation

All functions are documented and multiple examples that reproduce some informative results already published in literature are available in the online manual [19].

4. Examples

In this section we discuss a few examples to show how UNDI can be used in conjunction with *ab inito* methods to check or identify muon sites in crystals or to predict experimental features.

4.1. Copper

As a first very simple example, let us consider the calculation of the polarization function of a muon in the octahedral void of FCC Copper. We would like to compare the exact result, which includes Cu-Cu dipolar interactions, to the approximated one, originally obtained by Celio [11, 20], where the dipolar interaction between the nuclei has to be neglected.
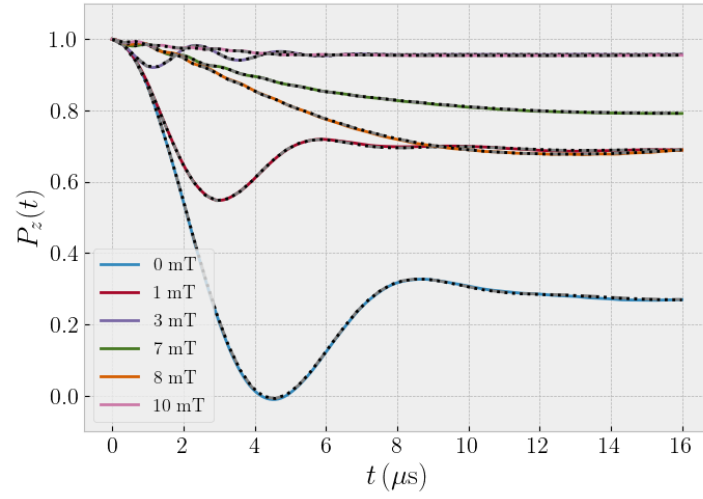
Figure 2: Muon spin polarization along the [111] direction for a Cu FCC crystal as a function of time for various applied longitudinal fields reported in the legend. The exact results obtained including (black dotted lines) or exluding (gray dash-dotted lines) Cu-Cu dipolar interaction are compared with the approximated ones (continuous lines). Cu atoms occupy a position with cubic symmetry and the EFG is actually generated by the muon. Four repetitions of the approximated algorithm were used in this case.

The Hilbert space is 8192 dimensional and therefore it can also be treated exactly on modern personal computers. In Fig. 2 the expected muon polarization is obtained for the initial spin polarization **s** of the muon aligned with the [111] direction of a single crystal sample and an external longitudinal field with values ranging from 0 to 10 mT is applied. The exact and approximated methods are compared. The results show minimal discrepancies and the ALCR occurring at about 8 mT is clearly visible.

Notably, in this case the small EFG generated by the muon becomes clearly detectable owing to the fact that in bulk copper Cu occupies a site of cubic symmetry and the EFG is zero by symmetry. Since accurate computational estimates of the EFG produced by the muon have been reported already 40 years ago [21, 22] there is little interest in reproducing those results here and therefore we move to more interesting cases.

4.2. MnSi

A more involved example is presented using MnSi as a test case [20, 23, 24]. The magnetic order and the muon site in this compound have been meticulously described in a number of recent publications, that have eventually clarified the uncertainty related to the presence of two interstitial muon sites [20]. Multiple experimental and computational evidences have confirmed that only a single muon site is occupied in the sample, differently from previous indications [25].

Here we give yet another confirmation of the position of the muon site based on the dipolar interaction between the muon and Mn atoms in the sample. In order to do so the EFG at Mn sites must be estimated in first place and we opt for using Density Functional Theory (DFT) implemented with a full-electron basis set. The details of the simulations are given in the appendix. In the principal axis system, V_{zz}^{PARA} is estimated to be $1.6\,10^{21}\mathrm{V/m^2}$ for the spin-degenerate case while it decreases to $V_{zz}^{FM} = 3.1\,10^{20}\mathrm{V/m^2}$ when a ferromagnetic order, resembling the low temperature and long wavelength helical order, is considered providing reasonable good agreement with the estimate available in literature [26] and showing the substantial role of spin degrees of freedom. Indeed it is worthwhile to mention that the EFG was unexpectedly found to be temperature dependent. This was understood to be a consequence of the coupling between charge-density and spin-density fluctuations explained by Takahashi and Moriya [27].

Fig. 3 compares the predicted polarization function of the muon using the known muon site [28, 29, 30] and the bulk EFG estimated in this work
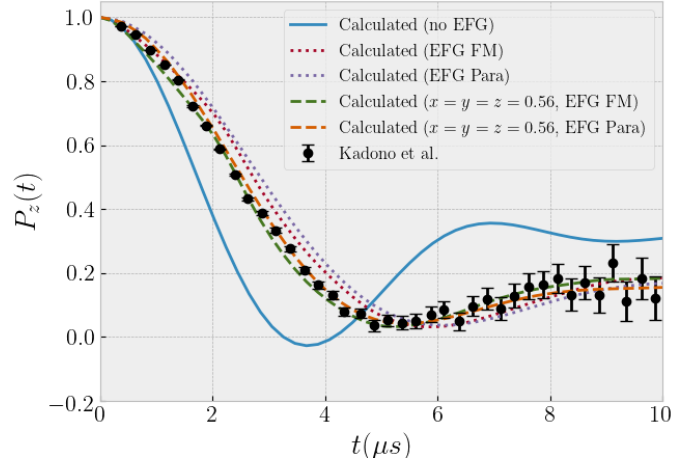
Figure 3: Expected muon polarization in presence (absence) of the EFG on Mn atoms in MnSi obtained from both a ferromagnetic and a paramagnetic electronic state. In the simulation Mn is in (0.138,0.138,0.138) while the known muon site has fractional coordinates (0.532, 0.532, 0.532). When considering only the bulk EFG as estimated from DFT, the best agreement with the experiment is obtained with a muon position slightly closer to the three nearest neighbouring Mn nuclei, namely (0.56, 0.56, 0.56).

(both FM and spinless case), with the experimental data taken at 150 K published in Ref [20]. While the curve obtained without taking into account the quadrupolar interaction drastically overestimates the depolarization, a better agreement is found when adding the bulk EFG. A small but noticeable deviation still exists. This is partially due to the discrepancy between the *ab initio* and the experimental EFG, but predominantly arises from the neglected contribution originating from the muon, which has been shown to be a small perturbation by comparison of the μSR and NMR data [20], but will break the symmetry of the EFGs at the Mn sites. We mention that a perfect agreement is recovered by shifting the muon position slightly closer to the nearest neighbouring Mn atoms, thus proving an estimate of the accuracy based only on the data from the unperturbed crystal.

Interestingly, the zero field polarization function can also be used to identify the possible muon sites. This has been attempted for example in $La_{2-x}Sr_xCuO_4$ [31], starting from the previous knowledge of a handful of possible muon sites.

Here we compute instead the expected signal for a grid of $10 \times 10 \times 10$ positions in the unit cell. While faster options are available [2], this example shows that arbitrarily accurate quantum simulations as implemented in UNDI can already be used to this aim. Indeed the whole simulation, that also requires powder averages, takes a few hours on a single core of a consumer level laptop.

In order to find the candidate sites we calculate the sum of the squared deviations between the experimental points of Fig. 3 and the calculated signal for each position of the grid in the time window between 0 and 5 μs. Each simulation is performed by searching for the nearest neighboring Mn nuclei up to 1.6 times the shortest bond length (roughly corresponding to a 1/4 ratio between the strength of the dipolar interaction for the nearest and the farthest Mn nucleus) or up to 5 nearest neighbours. The convergence of the Celio method is checked at runtime for each point and the powder average is performed with the method of Ref. [32][3]. Interstitial positions closer than 1 Å to Mn or Si atoms are rejected.

The set of positions that best reproduce the experimental signal are shown

---

[2]For example, it has been shown that for sufficiently large spins a classical approach is accurate enough and very efficient. Alternatively, the secular approximation can be used to estimate the second moment of the field distribution causing the depolarization.

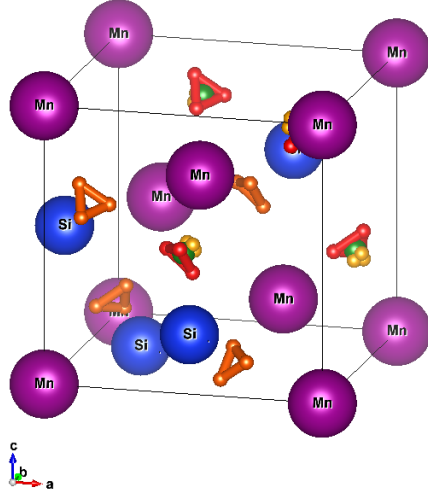[3]The implementation available in Ref. [33] was actually used.

Figure 4: Set of points providing the best agreement with the experimentally measured zero field μSR data in MnSi. The color code from yellow to red reflects best to worse match. The green sphere is the known muon site.

in Fig. 4 where we only add the points that have up to twice the best sum of square deviations from the experimental data. The known muon position is also visible as a green sphere. Two interstitial positions are found to be compatible with the zero field μSR observations: the best match is found with interstitial points shown in yellow, very close to the known muon site, while a second set of points (orange) lies just slightly more than 1 Å far from Si atoms. This second best match is unlikely to be present given the short muon to Si distance. A third set of points (red) is again located close to the known muon site.

Incidentally, similar results and conclusions were obtained in Ref. [25], which however required a single crystal sample and a number of transverse field measurements.

4.3. CeB_6

The magnetic and electronic ordering of CeB_6 is still matter of study about 40 years after the first characterizations [34, 35, 36, 37, 38, 39, 40, 41]. More precisely, the nature of an antiferroquadrupolar (AFQ) order taking
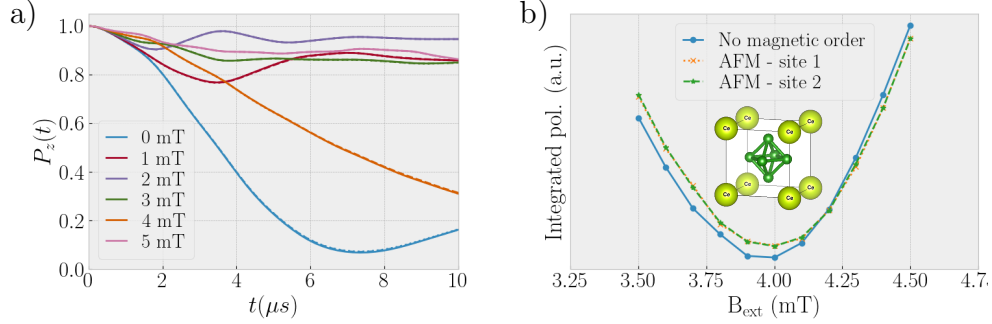
Figure 5: In a) zero field and longitudinal field muon spin polarization in CeB$_6$, with the initial muon polarization along the [111] direction. The EFG at B sites is obtained from DFT. The dotted and dashed lines, barely visible, show the signal from the symmetry equivalent sites. These lines should overlap perfectly and the deviations are a measure of the convergence of the algorithm. In b) the ALCR is shown as a dip in the integrated polarization as a function of applied field. The continuous line is obtained from the simulations shown in a), where the EFG on ^{11}B is from the first principles simulation performed without the spin degrees of freedom. The dashed and dotted lines are generated from the muons a two interstitial sites made inequivalent by the the antiferromagnetic ordered discussed in [46].

place at T_Q, a few K above a first-order magnetic transition, is still a matter of debate [42, 43, 44, 45]. In a recently published letter [46], Barman *et al.* propose that an orbital-ordered AFQ state originates from crystal field splitting and spin-orbit coupling. Kadono *et al.* [47] tried in vain to probe the AFQ transition by collecting longitudianl field μSR data aiming at a precise determination of the EFG on B atoms above and below T_Q that was instead shown to be insensitive to the transition.

The muon site in this compound[4] has been reported to be in the middle of the line joining Ce atoms (see inset of Fig. 5b). UNDI can be used to verify this result, but since the possibility to identify muon positions has already been shown with the previous example, we skip this task here.

We start instead by reproducing the ALCR using the EFG at B nuclei obtained with a simulation performed using the unit cell and disregarding the spin degree of freedom. The muon has 8 nearest neighbouring B nuclei that we consider entirely as ^{11}B, with spin 3/2. The approximated approach

---

[4]Also in this case the muon site was identified by estimating the muon interaction with the nuclear moments of the neighbouring B atoms in the paramagnetic phase

is mandatory in this case and a single repetition is sufficient to converge the algorithm. The ALCR is expected to happen at $B_{ext} \sim 3.8$ mT from NMR estimates [48, 37] of B EFG while, using the *ab initio* estimate, we observe it at about 4 mT (Fig. 5).

Using the prescriptions of Ref. [46], described in the appendix, with a full potential DFT approach we do properly obtain an antiferromagnetic ground state with 0.7 μ_B magnetic moment on Ce atoms, but the consequent electronic charge distribution differs from the one presented by in the original reference [46]. The modulation of the EFG on B nuclei is tiny and the overall change is also very small. This is shown in Fig. 5b where the difference in the ALCR obtained from the two electronic states is close to the sensitivity of the experimental technique, thus in agreement with the experimental findings [47]. A further exploration of the electronic states of CeB_6 and their effect on ALCR μSR experiments is beyond the scope of this paper and is left for future work.

5. Conclusions

We have presented UNDI, a tool for simulating the muon polarization function originating from the dipolar interaction between the muon and the nuclei in crystalline materials. The tool has a rich yet easy and intuitive input syntax that allows to describe the details of the sample under study either obtained experimentally or with computational approaches.

With the help of a few examples we have shown the potentialities of this software for μSR data analyses, especially when combined with *ab initio* based estimates of EFGs, which are, in general, easier to obtain than hyperfine coupling constants [49, 50].

The examples also served as a bird's eye view on the multiple potentialities of an accurate analysis of muon nuclear interactions for the determination of the physical properties of the sample under the study, such as the disentanglement of magnetic interactions of electronic and nuclear origin or the accurate estimation of the influence of charge ordered states on μSR signals.

For these reasons, UNDI is a precious companion to standard μSR data analyses.

6. Acknowledgments

Appendix

The details of first principles simulations discussed in this paper are summarized in the following paragraph.

All simulations where performed with the full-potential linearised augmented-plane wave code Elk [51]. The `highq` option was always set and a Monkhorst-Pack grid of $8 \times 8 \times 8$ points was used for MnSi and the unit cell of CeB_6. The $2 \times 2 \times 2$ supercell of CeB_6 was simulated with the standard accuracy parameters of the Elk code, but using a ratio between empty and valence states of 29% and a highly refined $7 \times 7 \times 7$ Monkhorst-Pack grid. Following [46], we set up an antiferromagnetic state with propagation vector $(\frac{1}{2}, \frac{1}{2}, \frac{1}{2})$ using two inequivalent Ce atoms and enforcing f electrons' localization with DFT+U [52], with a Hubbard U=3 eV and J=1 eV.

Convergence with respect to the spherical orbital expansion of the inner part of the muffin tin was checked and `lmaxi=3` was set in all cases. All simulations were performed with the Perdew-Burke-Ernzerhof exchange and correlation functional [53].

References

[1] K. Nagamine, Introductory Muon Science, Cambridge University Press, 2003.

[2] S. N. A. Ahmad, S. Sulaiman, D. F. H. Baseri, L. S. Ang, N. Z. Yahaya, H. Arsad, I. Watanabe, Density functional theory studies of muon stopping sites and hyperfine interaction in [au25(sr)18]0 nanocluster, J. Phys. Soc. Jpn. 89 (1) (2020) 014301. arXiv:https://doi.org/10.7566/JPSJ.89.014301, doi:10.7566/JPSJ.89.014301.
URL https://doi.org/10.7566/JPSJ.89.014301

[3] L. Liborio, S. Sturniolo, D. Jochym, Computational prediction of muon stopping sites using ab initio random structure searching (airss), J. Chem. Phys. 148 (13) (2018) 134114. arXiv:https://doi.org/10.1063/1.5024450, doi:10.1063/1.5024450.
URL https://doi.org/10.1063/1.5024450

[4] B. M. Huddart, M. T. Birch, F. L. Pratt, S. J. Blundell, D. G. Porter, S. J. Clark, W. Wu, S. R. Julian, P. D. Hatton, T. Lancaster, Local magnetism, magnetic order and spin freezing in the 'nonmetallic metal' FeCrAs, J. Phys. Condens. Matter 31 (28) (2019) 285803. `doi:10.1088/1361-648x/ab151f`.
URL `https://doi.org/10.1088%2F1361-648x%2Fab151f`

[5] K. J. A. Franke, B. M. Huddart, T. J. Hicken, F. Xiao, S. J. Blundell, F. L. Pratt, M. Crisanti, J. A. T. Barker, S. J. Clark, A. c. v. Štefančič, M. C. Hatnean, G. Balakrishnan, T. Lancaster, Magnetic phases of skyrmion-hosting $gav_4s_{8-y}se_y$ $(y = 0, 2, 4, 8)$ probed with muon spectroscopy, Phys. Rev. B 98 (2018) 054428. `doi:10.1103/PhysRevB.98.054428`.
URL `https://link.aps.org/doi/10.1103/PhysRevB.98.054428`

[6] T. Lancaster, F. Xiao, B. M. Huddart, R. C. Williams, F. L. Pratt, S. J. Blundell, S. J. Clark, R. Scheuermann, T. Goko, S. Ward, J. L. Manson, C. Rüegg, K. W. Krämer, Quantum magnetism in molecular spin ladders probed with muon-spin spectroscopy, New J. Phys. 20 (10) (2018) 103002. `doi:10.1088/1367-2630/aae21a`.
URL `https://doi.org/10.1088%2F1367-2630%2Faae21a`

[7] F. Xiao, J. S. Möller, T. Lancaster, R. C. Williams, F. L. Pratt, S. J. Blundell, D. Ceresoli, A. M. Barton, J. L. Manson, Spin diffusion in the low-dimensional molecular quantum heisenberg antiferromagnet $Cu(pyz)(NO_3)_2$ detected with implanted muons, Phys. Rev. B 91 (2015) 144417. `doi:10.1103/PhysRevB.91.144417`.
URL `https://link.aps.org/doi/10.1103/PhysRevB.91.144417`

[8] F. K. K. Kirschner, R. D. Johnson, F. Lang, D. D. Khalyavin, P. Manuel, T. Lancaster, D. Prabhakaran, S. J. Blundell, Spin jahn-teller antiferromagnetism in $coti_2o_5$, Phys. Rev. B 99 (2019) 064403. `doi:10.1103/PhysRevB.99.064403`.
URL `https://link.aps.org/doi/10.1103/PhysRevB.99.064403`

[9] P. Bonfà, R. D. Renzi, Toward the computational prediction of muon sites and interaction parameters, J. Phys. Soc. Jpn. 85 (9) (2016) 091014. `doi:10.7566/jpsj.85.091014`.
URL `https://doi.org/10.7566%2Fjpsj.85.091014`

[10] G. Luke, Quantum diffusion and spin dynamics of muons in copper, Ph.D. thesis, University of British Columbia (1988). `doi:http://dx.doi.org/10.14288/1.0085012`.
URL `https://open.library.ubc.ca/collections/ubctheses/831/items/1.0085012`

[11] M. Celio, New method to calculate the muon polarization function, Phys. Rev. Lett. 56 (1986) 2720–2723. `doi:10.1103/PhysRevLett.56.2720`.
URL `https://link.aps.org/doi/10.1103/PhysRevLett.56.2720`

[12] A. Yaouanc, P. de Réotier, Muon Spin Rotation, Relaxation, and Resonance: Applications to Condensed Matter, International Series of Monogr, OUP Oxford, 2011.

[13] S. F. J. Cox, Detection of quadrupole interactions by muon level crossing resonance, Zeitschrift für Naturforschung A 47 (1-2) (1992) 371 – 381. `doi:https://doi.org/10.1515/zna-1992-1-263`.
URL `https://www.degruyter.com/view/journals/zna/47/1-2/article-p371.xml`

[14] S. van der Walt, S. C. Colbert, G. Varoquaux, The NumPy array: A structure for efficient numerical computation, Comput. Sci. Eng. 13 (2) (2011) 22–30. `doi:10.1109/mcse.2011.37`.
URL `https://doi.org/10.1109/mcse.2011.37`

[15] J. Johansson, P. Nation, F. Nori, Qutip: An open-source python framework for the dynamics of open quantum systems, Comput. Phys. Commun. 183 (8) (2012) 1760 – 1772. `doi:https://doi.org/10.1016/j.cpc.2012.02.021`.
URL `http://www.sciencedirect.com/science/article/pii/S0010465512000835`

[16] J. Johansson, P. Nation, F. Nori, Qutip 2: A python framework for the dynamics of open quantum systems, Comput. Phys. Commun. 184 (4) (2013) 1234 – 1240. `doi:https://doi.org/10.1016/j.cpc.2012.11.019`.
URL `http://www.sciencedirect.com/science/article/pii/S0010465512003955`

[17] mendeleev – a python resource for properties of chemical elements, ions and isotopes, ver. 0.3.6, `https://github.com/lmmentel/mendeleev` (2014–).

[18] J. H. Brewer, S. R. Kreitzman, D. R. Noakes, E. J. Ansaldo, D. R. Harshman, R. Keitel, Observation of muon-fluorine "hydrogen bonding" in ionic crystals, Phys. Rev. B 33 (1986) 7813–7816. `doi:10.1103/PhysRevB.33.7813`.
URL `https://link.aps.org/doi/10.1103/PhysRevB.33.7813`

[19] P. Bonfà, UNDI Documentation, `https://undi.readthedocs.io/`, [Online; accessed 19-July-2020] (2020).

[20] R. Kadono, T. Matsuzaki, T. Yamazaki, S. R. Kreitzman, J. H. Brewer, Spin dynamics of the itinerant helimagnet mnsi studied by positive muon spin relaxation, Phys. Rev. B 42 (1990) 6515–6522. `doi:10.1103/PhysRevB.42.6515`.
URL `https://link.aps.org/doi/10.1103/PhysRevB.42.6515`

[21] P. Jena, S. G. Das, K. S. Singwi, Electric-field gradient at cu nuclei due to an interstitial positive muon, Phys. Rev. Lett. 40 (1978) 264–266. `doi:10.1103/PhysRevLett.40.264`.
URL `https://link.aps.org/doi/10.1103/PhysRevLett.40.264`

[22] H. Teichler, Microscopic calculation of lattice distortions around $\mu+$ in cu, Physics Letters A 67 (4) (1978) 313 – 315. `doi:https://doi.org/10.1016/0375-9601(78)90315-8`.
URL `http://www.sciencedirect.com/science/article/pii/0375960178903158`

[23] I. M. Gat-Malureanu, A. Fukaya, M. I. Larkin, A. J. Millis, P. L. Russo, A. T. Savici, Y. J. Uemura, P. P. Kyriakou, G. M. Luke, C. R. Wiebe, Y. V. Sushko, R. H. Heffner, D. E. MacLaughlin, D. Andreica, G. M. Kalvius, Field dependence of the muon spin relaxation rate in mnsi, Phys. Rev. Lett. 90 (2003) 157201. `doi:10.1103/PhysRevLett.90.157201`.
URL `https://link.aps.org/doi/10.1103/PhysRevLett.90.157201`

[24] R. S. Hayano, Y. J. Uemura, J. Imazato, N. Nishida, T. Yamazaki, R. Kubo, Zero-and low-field spin relaxation studied by positive muons,

Phys. Rev. B 20 (1979) 850–859. `doi:10.1103/PhysRevB.20.850`.
URL `https://link.aps.org/doi/10.1103/PhysRevB.20.850`

[25] A. Amato, P. Dalmas de Réotier, D. Andreica, A. Yaouanc, A. Suter, G. Lapertot, I. M. Pop, E. Morenzoni, P. Bonfà, F. Bernardini, R. De Renzi, Understanding the μsr spectra of mnsi without magnetic polarons, Phys. Rev. B 89 (2014) 184425. `doi:10.1103/PhysRevB.89.184425`.
URL `https://link.aps.org/doi/10.1103/PhysRevB.89.184425`

[26] H. Yasuoka, V. Jaccarino, R. C. Sherwood, J. H. Wernick, NMR and susceptibility studies of MnSi aboveTc, J. Phys. Soc. Jpn. 44 (3) (1978) 842–849. `doi:10.1143/jpsj.44.842`.
URL `https://doi.org/10.1143/jpsj.44.842`

[27] Y. Takahashi, T. Moriya, Effect of spin fluctuations on the electric field gradient in itinerant electron magnets, J. Phys. Soc. Jpn. 44 (3) (1978) 850–858. `arXiv:https://doi.org/10.1143/JPSJ.44.850`, `doi:10.1143/JPSJ.44.850`.
URL `https://doi.org/10.1143/JPSJ.44.850`

[28] A. Yaouanc, P. Dalmas de Réotier, B. Roessli, A. Maisuradze, A. Amato, D. Andreica, G. Lapertot, Dual nature of magnetism in mnsi, Phys. Rev. Research 2 (2020) 013029. `doi:10.1103/PhysRevResearch.2.013029`.
URL `https://link.aps.org/doi/10.1103/PhysRevResearch.2.013029`

[29] P. D. de Réotier, A. Yaouanc, A. Amato, A. Maisuradze, D. Andreica, B. Roessli, T. Goko, R. Scheuermann, G. Lapertot, On the robustness of the MnSi magnetic structure determined by muon spin rotation, Quantum Beam Science 2 (3) (2018) 19. `doi:10.3390/qubs2030019`.
URL `https://doi.org/10.3390/qubs2030019`

[30] R. Kadono, J. H. Brewer, K. Chow, S. R. Kreitzman, C. Niedermayer, T. M. Riseman, J. W. Schneider, T. Yamazaki, Critical behavior of electric field gradient in MnSi studied by muon level-crossing resonance, Hyperfine Interact. 85 (1) (1994) 259–264. `doi:10.1007/bf02069431`.
URL `https://doi.org/10.1007/bf02069431`

[31] W. Huang, V. Pacradouni, M. P. Kennett, S. Komiya, J. E. Sonier, Precision search for magnetic order in the pseudogap regime of $la_{2-x}sr_xcuo_4$ by muon spin relaxation, Phys. Rev. B 85 (2012) 104527. `doi:10.1103/PhysRevB.85.104527`.
URL `https://link.aps.org/doi/10.1103/PhysRevB.85.104527`

[32] D. W. Alderman, M. S. Solum, D. M. Grant, Methods for analyzing spectroscopic line shapes. nmr solid powder patterns, J. Chem. Phys. 84 (7) (1986) 3717–3725. `arXiv:https://doi.org/10.1063/1.450211`, `doi:10.1063/1.450211`.
URL `https://doi.org/10.1063/1.450211`

[33] Soprano - A library developed by the CCP for NMR Crystallography, `https://ccp-nc.github.io/soprano/`, [Online; accessed 19-July-2020] (2020).

[34] R. Feyerherm, A. Amato, F. Gygax, A. Schenck, Y. Ōnuki, N. Sato, Problems of the magnetic structure of ceb6, Journal of Magnetism and Magnetic Materials 140-144 (1995) 1175 – 1176, international Conference on Magnetism. `doi:https://doi.org/10.1016/0304-8853(94)01281-4`.
URL `http://www.sciencedirect.com/science/article/pii/0304885394012814`

[35] O. Zaharko, P. Fischer, A. Schenck, S. Kunii, P.-J. Brown, F. Tasset, T. Hansen, Zero-field magnetic structure in ceb_6 reinvestigated by neutron diffraction and muon spin relaxation, Phys. Rev. B 68 (2003) 214401. `doi:10.1103/PhysRevB.68.214401`.
URL `https://link.aps.org/doi/10.1103/PhysRevB.68.214401`

[36] F. Gygax, A. Schenck, Dynamics of positive muons in cab6, Journal of Alloys and Compounds 404-406 (2005) 360 – 364, proceedings of the 9th International Symposium on Metal-Hydrogen Systems, Fundamentals and Applications (MH2004). `doi:https://doi.org/10.1016/j.jallcom.2004.12.161`.
URL `http://www.sciencedirect.com/science/article/pii/S0925838805008467`

[37] M. Kawakami, H. Bohn, H. Lütgemeier, S. Kunii, T. Kasuya, NMR study of a CeB6 single crystal in high magnetic field, Journal of Mag-

netism and Magnetic Materials 31-34 (1983) 415–416. `doi:10.1016/0304-8853(83)90301-3`.
URL `https://doi.org/10.1016/0304-8853(83)90301-3`

[38] S. V. Demishev, A. V. Semeno, A. V. Bogach, N. A. Samarin, T. V. Ishchenko, V. B. Filipov, N. Y. Shitsevalova, N. E. Sluchanko, Magnetic spin resonance in ceb_6, Phys. Rev. B 80 (2009) 245106. `doi:10.1103/PhysRevB.80.245106`.
URL `https://link.aps.org/doi/10.1103/PhysRevB.80.245106`

[39] M. Takigawa, H. Yasuoka, T. Tanaka, Y. Ishizawa, Nmr study on the spin structure of ceb6, J. Phys. Soc. Jpn. 52 (3) (1983) 728–731. `arXiv:https://doi.org/10.1143/JPSJ.52.728`, `doi:10.1143/JPSJ.52.728`.
URL `https://doi.org/10.1143/JPSJ.52.728`

[40] M. Kawakami, S. Kunii, K. Mizuno, M. Sugita, T. Kasuya, K. Kume, The 11b nuclear magnetic resonance in ceb6 single crystal, J. Phys. Soc. Jpn. 50 (2) (1981) 432–437. `arXiv:https://doi.org/10.1143/JPSJ.50.432`, `doi:10.1143/JPSJ.50.432`.
URL `https://doi.org/10.1143/JPSJ.50.432`

[41] F. N. Gygax, A. Schenck, G. Solt, O. Zaharko, Spin dynamics in ceb_6 studied by muon spin relaxation, Phys. Rev. B 81 (2010) 094434. `doi:10.1103/PhysRevB.81.094434`.
URL `https://link.aps.org/doi/10.1103/PhysRevB.81.094434`

[42] M. Amara, C. Opagiste, R.-M. Galéra, Retrieving ceb_6's lost magnetic entropy, Phys. Rev. B 101 (2020) 094411. `doi:10.1103/PhysRevB.101.094411`.
URL `https://link.aps.org/doi/10.1103/PhysRevB.101.094411`

[43] M. Amara, R.-M. Galéra, ceb_6 macroscopically revisited, Phys. Rev. Lett. 108 (2012) 026402. `doi:10.1103/PhysRevLett.108.026402`.
URL `https://link.aps.org/doi/10.1103/PhysRevLett.108.026402`

[44] T. Matsumura, T. Yonemura, K. Kunimori, M. Sera, F. Iga, Magnetic field induced $4f$ octupole in ceb_6 probed by resonant x-ray diffraction, Phys. Rev. Lett. 103 (2009) 017203.

doi:10.1103/PhysRevLett.103.017203.
URL https://link.aps.org/doi/10.1103/PhysRevLett.103.017203

[45] T. Matsumura, T. Yonemura, K. Kunimori, M. Sera, F. Iga, T. Nagao, J.-i. Igarashi, Antiferroquadrupole order and magnetic field induced octupole in ceb$_6$, Phys. Rev. B 85 (2012) 174417. doi:10.1103/PhysRevB.85.174417.
URL https://link.aps.org/doi/10.1103/PhysRevB.85.174417

[46] C. K. Barman, P. Singh, D. D. Johnson, A. Alam, Revealing the nature of antiferroquadrupolar ordering in cerium hexaboride: ceb$_6$, Phys. Rev. Lett. 122 (2019) 076401. doi:10.1103/PhysRevLett.122.076401.
URL https://link.aps.org/doi/10.1103/PhysRevLett.122.076401

[47] R. Kadono, W. Higemoto, A. Koda, K. Kakuta, K. Ohishi, H. Takagiwa, T. Yokoo, J. Akimitsu, Spin dynamics of $4f$ electrons in ceb$_6$ studied by muon spin relaxation, J. Phys. Soc. Jpn. 69 (10) (2000) 3189–3192. doi:10.1143/jpsj.69.3189.
URL https://doi.org/10.1143/jpsj.69.3189

[48] A. C. Gossard, V. Jaccarino, Boron nuclear magnetic resonance in rare earth intermetallic compounds, Proceedings of the Physical Society 80 (4) (1962) 877–881. doi:10.1088/0370-1328/80/4/309.
URL https://doi.org/10.1088/0370-1328/80/4/309

[49] I. J. Onuorah, P. Bonfà, R. D. Renzi, Muon contact hyperfine field in metals: A DFT calculation, Phys. Rev. B 97 (17). doi:10.1103/physrevb.97.174414.
URL https://doi.org/10.1103%2Fphysrevb.97.174414

[50] I. J. Onuorah, P. Bonfà, R. De Renzi, L. Monacelli, F. Mauri, M. Calandra, I. Errea, Quantum effects in muon spin spectroscopy within the stochastic self-consistent harmonic approximation, Phys. Rev. Materials 3 (2019) 073804. doi:10.1103/PhysRevMaterials.3.073804.
URL https://link.aps.org/doi/10.1103/PhysRevMaterials.3.073804

[51] The Elk Code, http://elk.sourceforge.net/.

[52] A. G. Petukhov, I. I. Mazin, L. Chioncel, A. I. Lichtenstein, Correlated metals and the $LDA + u$ method, Phys. Rev. B 67 (2003) 153106. `doi:10.1103/PhysRevB.67.153106`.
URL `https://link.aps.org/doi/10.1103/PhysRevB.67.153106`

[53] J. P. Perdew, K. Burke, M. Ernzerhof, Generalized gradient approximation made simple, Phys. Rev. Lett. 77 (1996) 3865–3868. `doi:10.1103/PhysRevLett.77.3865`.
URL `https://link.aps.org/doi/10.1103/PhysRevLett.77.3865`